

**ELECTROMAGNETIC SCATTERING BY ROUGH SURFACES WITH LARGE HEIGHTS AND SLOPES WITH APPLICATIONS TO MICROWAVE REMOTE SENSING OF ROUGH SURFACE OVER LAYERED MEDIA**

**D. Liang**

Electrical Engineering Department  
University of Washington  
185 Stevens Way, Paul Allen Center-Room AE100R, Seattle, WA, USA

**P. Xu**

Electronics Information School  
Wuhan University  
Luoshi Road, Wuhan, China

**L. Tsang and Z. Gui**

Electrical Engineering Department  
University of Washington  
185 Stevens Way, Paul Allen Center-Room AE100R, Seattle, WA, USA

**K. S. Chen**

National Central University of Taiwan  
Chung-Li, Taoyuan 320, Taiwan

**Abstract**—In this paper, we study the bistatic reflection and transmission properties of random rough surface with large slope and large height. Method of Moment (MOM) is used to solve the surface integral equations for 2D rough surface scattering problem. The modeled rough surfaces are similar to random rectangular grating, so that there are large slopes on the surface. The motivation of the study is to analyze scattering by sastrugi surface in Polar Regions. The ridges on the sastrugi surface have heights of about 20 cm. In microwave remote sensing of land at 5 GHz, 10 GHz, 19 GHz and 37 GHz, these heights are larger than wavelength. Next, we consider

---

Corresponding author: D. Liang (dingl@u.washington.edu).

the scattering problem of the sastrugi rough surface over multi-layered snow. The bistatic reflection and transmission coefficients from MOM solutions are used as the boundary conditions for multi-layered radiative transfer equations. The radiative transfer equations are solved and the reflectivities are calculated. Numerical results are illustrated as a function of roughness and multi-layered parameters. We demonstrate that rough surface of sastrugi, when interactions with layered media, causes increase in reflectivity and the decrease in emissivity. The increase of reflectivity can be attributed to the fact that rough surface with large slope facilitates large angle transmission. The large angle transmission results in increase of subsurface reflection and the possibility of total internal reflection in layered media below the rough surface.

## 1. INTRODUCTION

Sastrugi are wind induced azimuth asymmetric rough surface with ridges parallel to the prevailing winds. At Greenland summit, sastrugi amplitudes are approximately 20 cm and the profiles exhibited abrupt geometries on slopes in later winter [1]. The top of sastrugi are relatively flat. In microwave remote sensing, WindSat data has shown microwave reflectivities are high over sastrugi region for the vertical and horizontal brightness temperatures [2]. In a recent paper, we consider emissivities of all four Stokes parameters using a coherent approach of rough surface scattering from a periodic surface over layered medium [3].

In this paper, we study the problem using a two-step approach. In the first step, we first study the bistatic reflection and transmission properties of random rough surface with large slope and large height by solving surface integral equations. In this paper, the modeled rough surfaces are similar to random rectangular grating, so that there are large slopes on the surface. In the second step, we consider the scattering problem of the sastrugi rough surface over multi-layered snow. We assume that the wave interactions between the layered snow and the sastrugi rough surface are incoherent, The reflections from sastrugi over layered snow is obtained by solving multilayer radiative transfer (RT) equations The bistatic reflection and transmission coefficients of sastrugi calculated in the first step are used as the boundary conditions for the radiative transfer equations in the second step. The radiative transfer equations are solved and the reflectivities are calculated.

We use numerical solution of Maxwell equations to obtain bistatic

transmission coefficient of half space sastrugi. The wave equations for rough surface scattering are solved by using surface integral equations and the method of moments (MOM). Fast solver of UV method is used [4] to ensure the numerical accuracy of the calculation; the rough surface is discretized along the surface instead of horizontal direction. The rooftop basis function and Galerkin's method are used in MOM. After solving the wave equations numerically, we calculate the surface fields, the bistatic reflection and transmission are calculated from the surface fields.

The simulation results show that transmissivity for sastrugi alone have not much difference from that of smooth surface. However the sastrugi transmission angle can be much larger from that of smooth surface especially when sastrugi has large slope and large height. So when the transmitted wave impinges on the boundary below, total internal reflection can occur if the medium below has small permittivity. Total internal reflection leads to larger reflectivity and smaller emissivity compared to those of smooth surface. Thus the larger reflectivity and smaller emissivity are the effects from the wave interactions of sastrugi and snow layering structure. Frequency dependence of transmissivity is also studied for sastrugi surface.

The salient features of the results are that the reflectivities of sastrugi surface over layered media are larger than that of smooth surface over layered media. The reflectivity of sastrugi half space is small. The reflectivity of layered media is larger due to the reflections from layering. However, the wave interaction of sastrugi surface over layered media drastically increases the reflectivity.

## 2. ROUGH SURFACE GENERATION

Sastrugi is formed by strong winds depositing dense snow above light snow. The top crust has a larger density than snow underneath. Florent studied the stratigraphy of sastrugi in Arctic [5]. Lytle studies the snow permittivity and grain size of snow samples from 0.3m to 2.7m below the surface of Greenland ice sheet [6]. Albert and Hawley [1] studied seasonal changes in snow surface roughness at Summit, Greenland. Fig. 1 is the measured roughness profile on Feb. 27th, 1998. The dark curve has averaged height of 16 cm and *rms* height of 5.6 cm. Another one has averaged height of 5.3 cm and *rms* height of 3.3 cm. Combining the two together gives an averaged height of 11 cm and *rms* height is 7.1 cm. Fig. 2 is the histogram of the slope of the curves in Fig. 1. More than 5% of the slope is large than 55 degrees. We use the following method to generate realizations of random rough surface profiles.

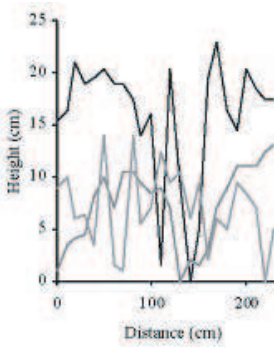


**Figure 1.** Measured Greenland Summit snow surface profile.

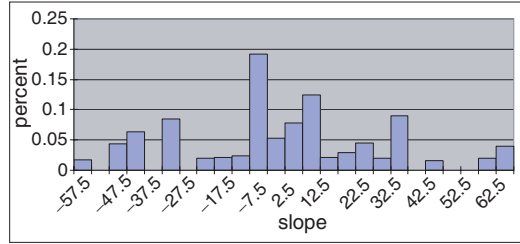


**Figure 2.** Histogram of the slope of profiles shown in Fig. 1.

Let  $N$  be the number of ridges on a length  $L$  along the  $x$  axis.  $H$  is the height of the ridges. The max slope is  $\alpha$  degrees. In the numerical simulation, we discretize the profile along the length with step of  $dl$ . A smooth curve connects the slope and flat part. Let  $\theta_1, \theta_2, \dots, \theta_m$  be the group of slopes of the curve which gradually change from  $\alpha$  degree to 0 degree. Fig. 3(a) illustrates the simulated sastrugi profile for  $m = 3$ , red section has the max slope. Then the height of the curve is  $\sum_{i=1}^m (dl \cdot \sin \theta_i)$ , and the length of the curve along the  $x$  axis is  $\sum_{i=1}^m (dl \cdot \cos \theta_i)$ . The height of the  $\alpha$  degree slope is  $H - 2 \sum_{i=1}^m (dl \cdot \sin \theta_i)$ , and the length of the  $\alpha$  degree slope along the  $x$  axis is  $(H - 2 \cdot \sum_{i=1}^m (dl \cdot \sin \theta_i)) / \tan(\alpha)$ . Generate two groups of independent positive random numbers  $\{a'_1, a'_2, \dots, a'_N\}$  with mean value of  $\bar{a}'$ , and  $\{b'_1, b'_2, \dots, b'_{N+1}\}$  with mean value of  $\bar{b}'$ . Let  $a_i = a'_i \cdot C$  be the length of the top of the  $i$ th ridges and  $b_i = b'_i \cdot C$ , be the length of the  $i$ th grooves.  $C$  can be calculated from the equation of the total length of the ridges and grooves:

$$\left( \sum_{i=1}^N a'_i + \sum_{i=1}^{N+1} b'_i \right) C = L - 2N \cdot \left( H - 2 \cdot \sum_{i=1}^m (dl \cdot \sin \theta_i) \right) / \tan(\alpha) - 4N \cdot \sum_{i=1}^m (dl \cdot \cos \theta_i) \quad (1)$$

The averages height of the rough surface is

$$\langle h \rangle = \left[ 2N \cdot \left( H - 2 \cdot \sum_{i=1}^m (dl \cdot \sin \theta_i) \right) / \tan(\alpha) + 4N \cdot \sum_{i=1}^m (dl \cdot \cos \theta_i) + C \sum_{i=1}^N a'_i \right] / L \quad (2)$$

If the slope is 85 degrees, the averages height of the rough surface is

$$\langle h \rangle = \frac{H \cdot N \cdot C\bar{a}' + \frac{H}{2} \cdot 2N \cdot H / \tan 85}{N \cdot C\bar{a}' + (N+1) \cdot C\bar{b}' + 2N \cdot H / \tan 85} \approx \frac{H \cdot N \cdot \bar{a}'}{N \cdot \bar{a}' + (N+1) \cdot \bar{b}'} \quad (3)$$

The *rms* height of the rough surface is

$$h_{rms} = \sqrt{E[h^2] - E[h]^2} \approx H \frac{\sqrt{N(N+1)\bar{a}' \cdot \bar{b}'}}{N\bar{a}' + (N+1)\bar{b}'}. \quad (4)$$

In this paper,  $\bar{a}' = \bar{b}'$  is used. We also use 12 ridges in a section of 15 m. The slope is 85 degrees and the height of the ridges is 19 cm. Then  $\langle h \rangle \approx 9.5$  cm and  $h_{rms} \approx 10$  cm. A realization of the sastrugi profile is shown in Fig. 3(b).

### 3. FORMULATIONS

We use rooftop basis functions and Galerkin's method to solve the surface integral equations associated with the rough surface scattering problem [7]. Let  $x$  be along the horizontal direction of the rough surface profile, and  $z$  is the height. Consider the incident plane wave with  $x$ - $z$  as the incident plane. The TM wave and TE wave are decoupled. For TM case when incident wave is from medium 0 with permittivity  $\varepsilon$  to medium 1 with permittivity  $\varepsilon_1$ , the integral equations are show below:

$$H_{inc}(x, z) + \int_{z'=f(x')} dS' [H(x', z') \hat{n}' \cdot \nabla g(x, z; x'z') - g(x, z; x'z') \hat{n}' \cdot \nabla H(x', z')] = \begin{cases} H(x, z), z > f(x) \\ 0, z < f(x) \end{cases} \quad (5a)$$

$$- \int_{z'=f(x')} dS' [H_1(x', z') \hat{n}' \cdot \nabla g_1(x, z; x'z') - g_1(x, z; x'z') \hat{n}' \cdot \nabla H_1(x', z')] = \begin{cases} 0, z > f(x) \\ H_1(x, z), z < f(x) \end{cases} \quad (5b)$$

Boundary conditions at  $z = f(x)$ , are

$$H(x, z) = H_1(x, z) \quad (6a)$$

$$\frac{1}{\varepsilon} \hat{n} \cdot \nabla H(x, z) = \frac{1}{\varepsilon_1} \hat{n} \cdot \nabla H_1(x, z) \quad (6b)$$

In the equation,  $\hat{n}$  is the normal direction of the surface  $z = f(x)$ ,  $g, g_1$  are 2-D green' function in media 0 and 1.

Imposing boundary condition and let

$$\psi(x, z) = H(x, z), \quad (7a)$$

$$u(x, z) = \sqrt{1 + (f'(x))^2} \hat{n} \cdot \nabla \psi(x, z) \quad (7b)$$

Note that  $(x', z')$  is on the surface with  $z' = f(x')$ .

The surface integral equations from (3a) and (3b), are

$$\psi_{inc}(x) + \int dx' \left[ \psi(x') \sqrt{1 + (f'(x'))^2} \frac{\partial}{\partial n'} g(x; x') - g(x; x') u(x') \right] = \psi(x) \quad (8a)$$

$$-\int dx' \left[ \psi(x') \sqrt{1 + (f'(x'))^2} \frac{\partial}{\partial n'} g_1(x; x') - g_1(x; x') \frac{\varepsilon_1}{\varepsilon} u(x') \right] = 0 \quad (8b)$$

We divide the rough surface into  $N$  equal intervals  $\Delta l$  along the length of the surface, the  $n$ th interval ended at  $x_n$ . Let the first interval start at  $x_0$ . The rooftop basis functions are

$$r_n(t) = \begin{cases} \frac{t-t_{n+1}}{t_n-t_{n+1}}, & t_{n+1} > t \geq t_n \\ \frac{t-t_{n-1}}{t_n-t_{n-1}}, & t_n > t > t_{n-1} \text{ when } N-1 > n > 1 \\ 0, & \text{elsewhere} \end{cases} \quad (9)$$

$$r_0(t) = \begin{cases} \frac{t-t_1}{t_0-t_1}, & t_1 > t > t_0 \\ 0, & \text{elsewhere} \end{cases} \quad (10)$$

$$r_N(t) = \begin{cases} \frac{t-t_{N-1}}{t_N-t_{N-1}}, & t_N > t > t_{N-1} \\ 0, & \text{elsewhere} \end{cases} \quad (11)$$

The surface unknowns can be represented using the basis function:

$$\psi(x) = \sum_n \psi_n r_n(x), \quad (12a)$$

$$u(x) = \sum_n u_n r_n(x), \quad (12b)$$

We use MOM to solve (8a) and (8b).

$$\begin{aligned} & \sum_n \psi_n \int dx r_m(x) r_n(x) \\ & - \sum_n \psi_n \int dx' r_n(x') \int dx r_m(x) \sqrt{1 + (f'(x'))^2} \frac{\partial}{\partial n'} g(x; x') \\ & + \sum_n u_n \int dx' r_n(x') \int dx r_m(x) g(x; x') = \int dx r_m(x) \psi_{inc}(x) \end{aligned} \quad (13a)$$

$$\begin{aligned} & \sum_n \psi_n \int dx' r_n(x') \int dx r_m(x) \sqrt{1 + (f'(x'))^2} \frac{\partial}{\partial n'} g_1(x; x') \\ & - \sum_n u_n \frac{\epsilon_1}{\epsilon} \int dx' r_n(x') \int dx r_m(x) g_1(x; x') = 0 \end{aligned} \quad (13b)$$

Written in matrix form:

$$\begin{bmatrix} \bar{\bar{A}} & \bar{\bar{B}} \\ \bar{\bar{A}}^{(1)} & \bar{\bar{B}}^{(1)} \end{bmatrix} \bullet \begin{bmatrix} \bar{u} \\ \bar{\psi} \end{bmatrix} = \begin{bmatrix} \bar{b} \\ 0 \end{bmatrix}, \quad (14)$$

where

$$\begin{aligned} \bar{u} &= [u_1, u_2, \dots, u_N]^T, \\ \bar{\psi} &= [\psi_1, \psi_2, \dots, \psi_N]^T \end{aligned} \quad (15)$$

$$\bar{\bar{A}}(m, n) = \int dx' r_n(x') \int dx r_m(x) g(x; x')$$

$$\begin{aligned} \bar{\bar{B}}(m, n) &= \int dx r_m(x) r_n(x) - \int dx' r_n(x') \\ & \quad - \int dx r_m(x) \sqrt{1 + (f'(x'))^2} \frac{\partial}{\partial n'} g(x; x') \end{aligned} \quad (16)$$

$$\bar{b}(m) = \int dx r_m(x) \psi_{inc}(x) \quad (17)$$

$$\bar{\bar{A}}^{(1)}(m, n) = -\frac{\epsilon_1}{\epsilon} \int dx' r_n(x') \int dx r_m(x) g_1(x; x') \quad (18)$$

$$\begin{aligned} \bar{\bar{B}}^{(1)}(m, n) &= \sum_n \psi_n \int dx r_m(x) \\ & \quad \int dx' r_n(x') \sqrt{1 + (f'(x'))^2} \frac{\partial}{\partial n'} g_1(x; x') \end{aligned} \quad (19)$$

In Eqs. (15) to (19), the integration on  $x$  axis is up to 22.5 m. The bistatic transmission and scattering coefficients can be calculated from surface unknowns. Eq. (20) is the bistatic scattering coefficients when incident wave is from medium 0.  $k$  is the wave number in medium 0 and  $g$  controls the tapering of the incident wave.

$$\gamma_{00}^r(\theta_t, \theta_0) = \frac{|\psi_s^{(N)}(\theta_t)|^2}{8\pi k g \cos \theta_0 \sqrt{\frac{\pi}{2}} \left[ 1 - \frac{1 + 2 \tan^2 \theta_0}{2k^2 g^2 \cos^2 \theta_0} \right]} \quad (20)$$

where

$$\psi_s^{(N)}(\theta_t) = \int_{z=f(x')} dx' [\psi(x') ik (\sin \theta_t f'(x') - \cos \theta_t) - u(x')] \exp(-ikx' \sin \theta_t - ikf(x') \cos \theta_t) \quad (21)$$

#### 4. NUMERICAL RESULTS OF CONVERGENCE AND VALIDATIONS

First, we show the convergence of the result with the variation of sampling points. At the frequency of 10.7 GHz, we sample the surface realization in Fig. 3(b) using steps of 0.1, 0.075, 0.05 and 0.0375 wavelength along the length of the surface, that is 0.28 cm, 0.21 cm, 0.14 cm and 0.105 cm respectively. The number of sampling points are

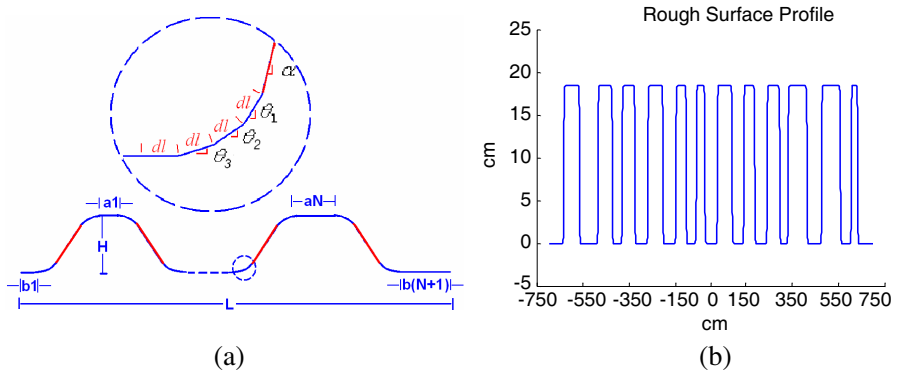


**Figure 3.** (a) Rough surface generation, (b) one realization of rough surface, length is 15 m and height is 18 cm.

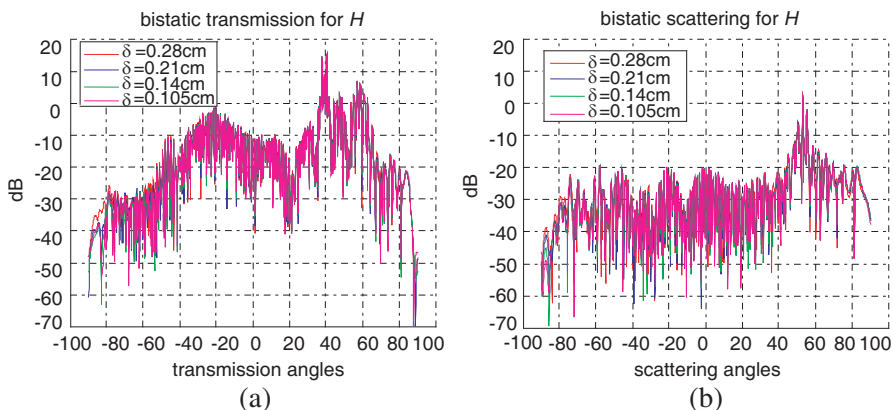


**Figure 4.** Bistatic coefficients for different discretizations for horizontal polarization. (a) Bistatic transmission coefficients, (b) Bistatic reflection coefficients.

**Table 1.** Energy conservation and emissivity for different discretizations.

	$dl$	Energy conservation	Emissivity	Reflectivity	Smooth surface
TE ( $H$ )	0.100	0.9940	0.9812	0.0128	0.9426
	0.075	0.9954	0.9708	0.0246	
	0.050	0.9953	0.9622	0.0331	
	0.0375	0.9962	0.9610	0.0352	
TM ( $V$ )	0.100	0.9893	1.0097	-0.0204	0.9999
	0.075	0.9929	1.0030	-0.0101	
	0.050	0.9945	0.9972	-0.0027	
	0.0375	0.9954	0.9954	0.0000	

6144, 8192, 12288 and 16384 respectively. Consider a wave impinging onto the rough surface from air. The incident wave is tapered by a factor of 3, incident angle is 53 degrees, and snow permittivity is 1.6. In Fig. 4 we compare the bistatic transmission and reflection for the single realization of the rough surface using the above 4 different sampling rates. Results show that bistatic coefficients have very small differences among different sampling rates, showing convergence with sampling.

In Table 1, we compare the energy conservation, transmissivity,

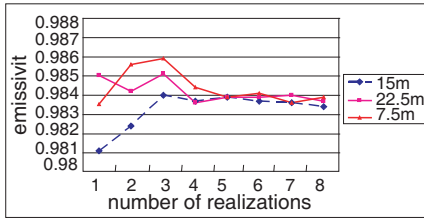


**Figure 5.** Emissivity averaged over maximum of 8 realizations for different length of rough surface from 7.5 m to 22.5 m, discretization is 0.28 cm.

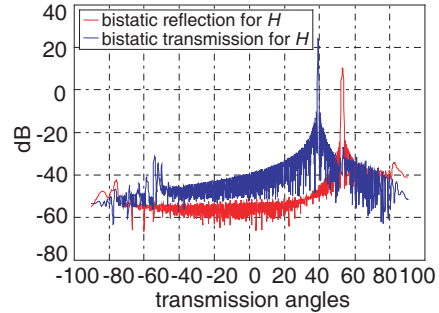


**Figure 6.** Bistatic coefficients for smooth surface.

and the transmissivity difference from that of a smooth surface for the 4 sampling rates. We note that better energy conservation is achieved using higher sampling rates. For the same sampling rate, energy conservation for  $H$ -pol is better than  $V$ -pol. Transmissivity converges as sampling rate increases for both  $H$ -pol and  $V$ -pol. Emissivity for  $V$ -pol is higher than  $H$ -pol because of the Brewster's angle. The simulated emissivity for  $V$ -pol is higher than 1 when sampling rate is not high enough. Emissivity for  $H$ -pol is larger than smooth surface, and emissivity for  $V$ -pol is smaller than smooth surface when sampling rate is high enough. Otherwise indicated we use  $dl = 0.28$  cm in the following part of the paper.

Next, we show the convergence with respect to realizations and with respect to surface lengths. Fig. 5 shows the emissivities for  $H$ -pol averaged over a maximum of 8 realizations for different rough surface lengths. The figure shows that simulated emissivity converges to around 0.984 after 5 realizations, and emissivity converges faster for longer surface. For 22.5 meters, the number of surface unknowns is 18432. In the following part of the paper, otherwise indicated, the rough surface length is 15 m. Simulated emissivities are averaged over 5 realizations.

We next show the validation of the simulation results by applying the MoM method to a smooth surface. The bistatic coefficients are shown in Fig. 6. There is only one transmission angle at 40 degrees and only one reflection angle at 53 degrees. Emissivity is 0.9405 for  $H$ -pol and 0.9987 for  $V$ -pol. These results agree with the Fresnel formulas and Snell's law.

## 5. NUMERICAL RESULTS OF HALF SPACE

We consider 2 scenarios: transmission from air to snow and from snow to air. We compare the bistatic coefficients and emissivity.

### 5.1. Transmission from Air to Snow

Figure 7 shows the bistatic transmission coefficients for  $H$ -pol when incident angle is 53 degrees. We compare three cases: a) height is 19 cm and maximum slope is 85 degrees, b) height is 19 cm and maximum slope is 60 degrees, and c) height is 6 cm and maximum slope is 85 degrees. We can also estimate the transmission angles by using geometric optics. When the slope is 85 degrees, the local incident angle on the slope is 32 degrees. Thus there are 2 major transmission

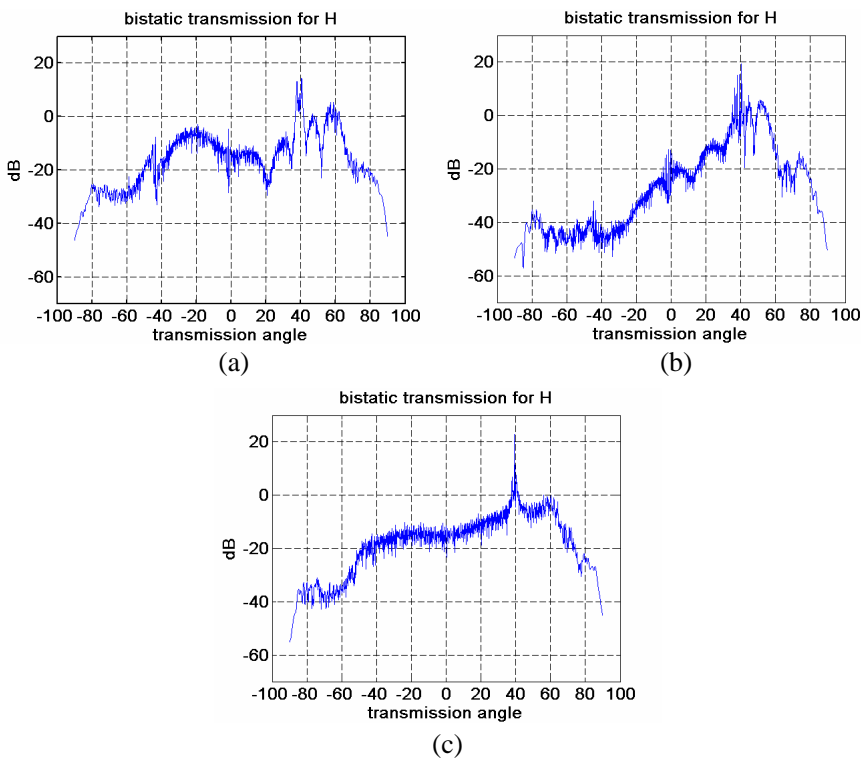


**Figure 7.** Bistatic transmission coefficients for  $H$ -pol, averaged after 5 realizations, incident angle is 53 degrees in air (a)  $H = 19$  cm, slope = 85, (b)  $H = 19$  cm, slope = 60, (c)  $H = 6$  cm, slope = 85.

angles. One is 40 degrees through the flat part. The other is 60 degrees for transmission through the slope. When slope is 60 degrees, the transmission angle through the slope is 54 degrees. From Fig. 7, we can identify the 2 major transmission angles. We also note that the transmission around 40 degrees is the largest because more energy is received and transmitted through flat part in the rough surface than through the slope. Fig. 7(a) shows stronger transmission at 60 degrees than that in Fig. 7(c) because the larger surface height allows more energy to be transmitted through the slope.

In Fig. 8, we compare the emissivities between rough surface and smooth surface. There is only a small difference between the emissivity of rough surface and that of smooth surface. In Table 2, we show the emissivities for two frequencies 10.7 GHz and 18.7 GHz. Sampling step is 0.05 free wavelength and 0.0874 wavelength in snow. The energy conservation at 10.7 GHz is better than at 18.7 GHz because sampling rate is higher for 10.7 GHz in terms of wavelength. The emissivity increases when frequency increases. The emissivity difference from

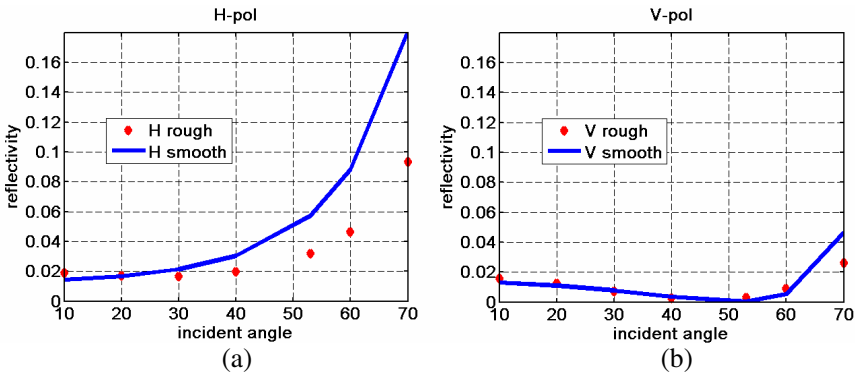


**Figure 8.** Comparison of reflectivity between half space sastrugi and smooth surface, incident wave is in air, permittivity of snow is 1.6.

**Table 2.** Frequency dependence of emissivity.

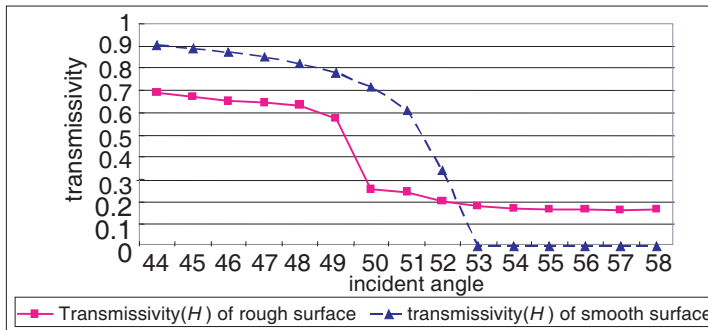
	freq	Energy conservation	Emissivity	Rough-Smooth	Smooth surface
TE (H)	10.7	0.9954	0.9635	0.0209	0.9426
	18.7	0.9949	0.9861	0.0435	
TM (V)	10.7	0.9946	0.9971	-0.0028	0.9999
	18.7	0.9933	1.0110	0.0111	

smooth surface increases for  $H$ -pol with the increase of frequency. Note that the  $V$ -pol has the Brewster angle effect and has higher emissivity than the  $H$ -pol even for smooth surface. However, the results indicate that the reflectivity for sastrugi surface over half space and smooth surface over half space are both small. The important effects of sastrugi surface are the much larger transmission angles due to the large slope.

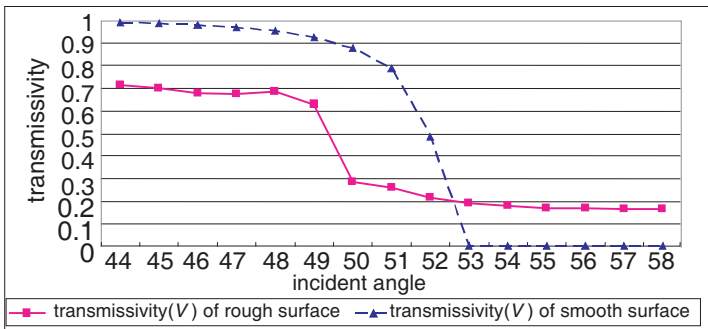
### 5.2. Transmission from Snow to Air

The sampling rate is 0.05 free wavelength corresponding to 0.0632 wavelength in snow with permittivity of 1.6. The surface length is still 15 m, which is longer in terms of wavelength than in the air. Emissivity and bistatic are averaged over 5 realizations.

In Fig. 9, we compare the emissivity between rough surface and smooth surface. The emissivity of rough surface is smaller than



(a)



(b)

**Figure 9.** Transmissivity from snow to air for smooth surface and sastrugi (a)  $H$ -pol, (b)  $V$ -pol.

smooth surface for small incident angles that are smaller than critical angle. When incident angle increases, emissivity from smooth surface and rough surface both decreases. The emissivity of smooth surface decreases to zero when incident angle exceeds the critical angle. However, the emissivity of rough surface shown is 0.2 instead of zero. At small incident angle, the local incident angle on the slope is larger than that on the flat part, so the total transmissivity of the rough surface is smaller than flat surface. When incident angle is larger, the local transmissivity on the slope is larger than that on the flat part of the rough surface because the local incident angle on the slope is smaller than that on the flat part. Hence the transmissivity of the rough surface is larger than that of flat surface. When the incident angle is larger than the critical angle, transmission of rough surface still exists because the local incident angle on the slope is smaller than the critical angle.

In Fig. 10(a), we compare the bistatic transmission coefficients for two different incident angles. The blue line has incident angle of 40 degrees which is less than critical angle of 53 degrees. The transmission angles are centered around 53 degrees. The red line has incident angle of 60 degrees that is larger than the critical angle. We see that there is still significant transmission when the incident angle is larger than the critical angle, this is because of the large slope in satrugi surface. In Fig. 10(b), we compare the bistatic scattering coefficients for incident angles of 40 and 60 degrees. We can see that scattering angles are centered around 40 degrees and 60 degrees respectively.

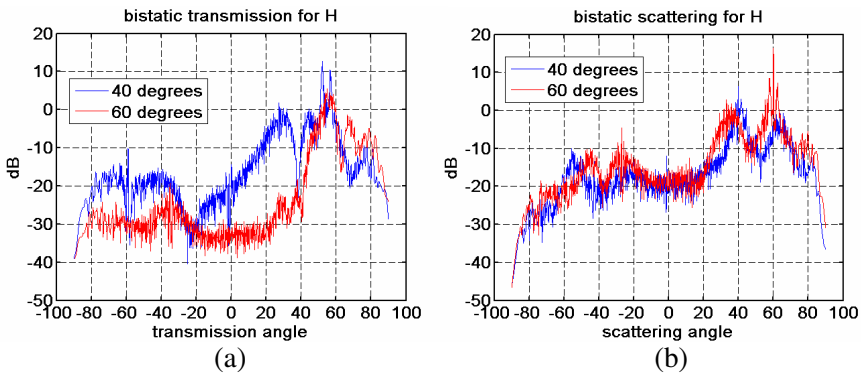


**Figure 10.** Bistatic coefficients from snow to air averaged over 5 realizations for horizontal polarization, incident angles are 40 degrees and 60 degrees. (a) Bistatic transmission coefficients, (b) Bistatic reflection coefficients.

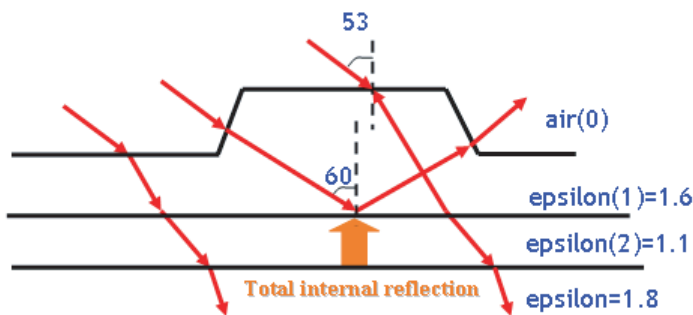


**Figure 11.** Wave propagation when incident from air to layered snow with sastrugi on top.

### 6. REFLECTIVITY FOR SASTRUGI OVER LAYERED SNOW

To analyze the reflectivity for sastrugi surface over layered snow, we solve the radiative transfer equations for active microwave remote sensing. We use the sastrugi bistatic scattering and transmission coefficients derived in previous sections as the boundary conditions. A layered snow profile is shown in Fig. 11. The bottom layer is a half space of snow. In the following radiative transfer equation,  $\kappa_a$  is absorption coefficient. The volume scattering is not considered because of small grain size [6]. In the boundary conditions  $\gamma_{11}^r(\theta_s, \theta_i)$  and  $\gamma_{01}^t(\theta_t, \theta_i)$  are the bistatic reflection coefficient and bistatic transmission coefficient when wave incident from layer 1 to air.  $\gamma_{00}^r(\theta_t, \theta_i)$  and  $\gamma_{10}^t(\theta_s, \theta_i)$  are the bistatic reflection coefficient and bistatic transmission coefficient when wave incident from air onto layer 1. Radiative transfer equations for layer 2 and below can be readily calculated and the combined effects are expressed in the effective reflectivity  $\bar{R}_g$  and transmissivity  $\bar{T}_g$  in the boundary condition at  $z = -d$ .  $\bar{I}(\theta_0, 0) = I_0\delta(\theta_0 - \theta_{0i})$  is the incident intensity.

$$\cos \theta \frac{d\bar{I}_u(\theta, z)}{dz} = -\kappa_a \bar{I}_u(\theta, z) \tag{22a}$$

$$-\cos \theta \frac{d\bar{I}_d(\theta, z)}{dz} = -\kappa_a \bar{I}_d(\theta, z) \tag{22b}$$

Boundary condition:

$$\text{At } z = -d, \bar{I}_u(\theta, -d) = \bar{R}_g \bar{I}_d(\theta, -d) \tag{23a}$$

$$\begin{aligned} \text{At } z = 0, \bar{I}_d(\theta_s, 0) \cos \theta_s = & \int_{-\pi/2}^{\pi/2} d\theta_i \bar{I}_u(\theta_i, 0) \gamma_{11}^r(\theta_s, \theta_i) \cos \theta_i \\ & + I_0 \gamma_{10}^t(\theta_s, \theta_0) \cos \theta_0 \end{aligned} \quad (23b)$$

The intensity in air is

$$\bar{I}_t(\theta_t, 0) \cos \theta_t = \int_{-\pi/2}^{\pi/2} d\theta_i \bar{I}_u(\theta_i, 0) \gamma_{01}^t(\theta_t, \theta_i) \cos \theta_i + I_0 \gamma_{00}^r(\theta_t, \theta_0) \cos \theta_0 \quad (24)$$

Reflectivity is

$$r = P_r/P_0 = \int_{-\pi/2}^{\pi/2} \bar{I}_t(\theta_t, 0) \cos \theta_t d\theta_t / I_0 \cos \theta_0 \quad (25)$$

In Fig. 12, we plot four snow profiles. These profiles are hypothetic, but realistic based on [5] and [6]. In profile (a), the first layer of snow has larger permittivity than the second layer. In profile (b), the first layer has smaller permittivity than the second layer. In profile (c), the first layer of snow has larger permittivity than the second layer; however, the permittivity contrast is not as large as in profile (a). In profile (d), there are more snow layers than the first three profiles. Then we simulate the reflectivity of these four profiles. In Fig. 13, the left, center and right figures show the reflectivity of Fig. 12(a) when kappaa is 1e-10/ cm, 1e-3/ cm, and

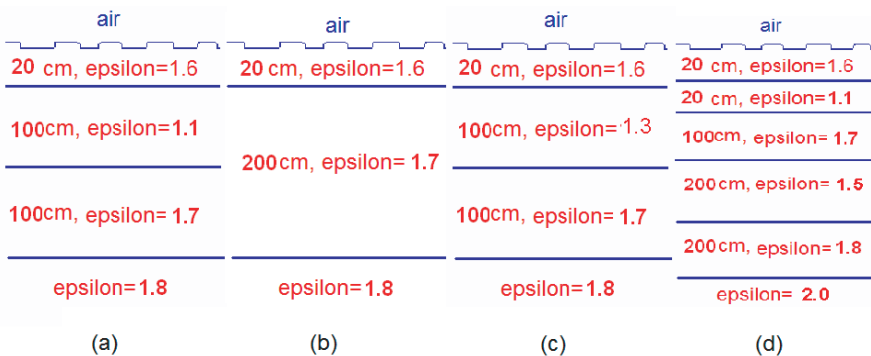


**Figure 12.** Sastrugi over layered snow profile.

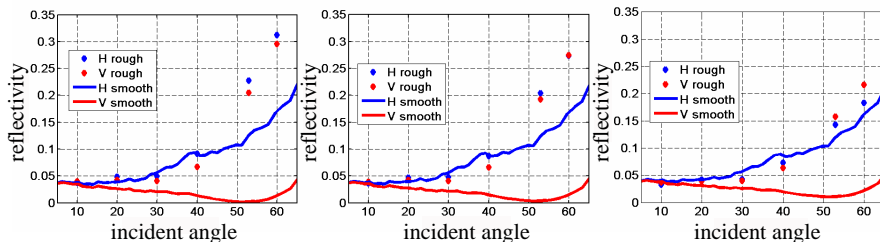


**Figure 13.** Reflectivity of Fig. 12(a) and smooth surface over the same layered snow. Kappaa is left: 1e-10/cm, center: 1e-3/cm, right: 5e-3/cm.

5e-3/cm respectively. In each figure the reflectivity of sastrugi over layered snow is compared with reflectivity of smooth surface over the same layered snow. Fig. 14 to Fig. 16 are the simulation results for Figs. 12(b) to (c) respectively. We note that from Figs. 13 to 15 the reflectivity of sastrugi over layered snow is comparable to smooth surface case when incident angle is smaller than 40 degrees. In Fig. 13, the reflectivity at *V* and *H* channel of sastrugi over layered snow is obviously larger than smooth surface case when the incident angles are larger than 50 degrees. From the bistatic transmission coefficient plot in Fig. 7(a), we find that when rough surface has maximum slope of 85 degrees and the ridges are high enough, and when incident angle is 53 degrees, the refraction angle with the second strongest transmission is at 60 degrees, which is refraction from the slope. 60 degrees is larger than the critical angle at the boundary below the rough surface. The so caused total internal reflection makes the reflectivity of sastrugi over layered snow significantly larger than that of the smooth surface. When the incident angle in air is small, the strong refraction angles in the snow layer below rough surface are still small; in this case, reflectivity of smooth surface layered snow and rough surface layered snow is comparable. We also note that in Fig. 7(b) when the slope is 60 degrees, the strong refraction angle is 53 degrees. In this case, the total internal reflection would occur for the strong refraction angle if the permittivity contrast between the first layer and other layers is large enough, that means if the permittivity of first layer is 1.6, the permittivity of layer below has to be less than 1.01, this is almost impossible for snow. Thus to make total internal reflection possible for Fig. 7(b), the permittivity of first layer has to be higher than 1.6. In Fig. 7(c), when the height of the ridges is not large enough, the transmission at large refraction angles, like 60 degrees, is very weak, thus the total internal reflection does not have much effect on reflectivity. So rough surface with large

slope and large height, along with enough permittivity contrast, are necessary conditions for total internal reflection to occur and increase of reflectivity. Fig. 13 also show that reflectivity decreases as absorption increases.  $H$ -pol decreases faster than  $V$ -pol. In the left figure  $H$  channel is larger than  $V$  channel and In the right figure  $H$  channel is smaller than  $V$  channel. The polarization difference of rough surface case is much smaller than smooth surface case.

In Fig. 14, we compare the reflectivity of profile Fig. 12(b) and the reflectivity of smooth surface over the same layered snow. For rough surface,  $V$  channel is larger than  $H$  channel.  $V$  channel rough surface reflectivity is larger than both  $H$  and  $V$  channel smooth surface reflectivity;  $H$  channel rough surface reflectivity is larger than  $V$  channel smooth surface reflectivity and smaller than  $H$  channel smooth surface reflectivity. As kappa change, there is no obvious change in reflectivity. Because the second layer has larger permittivity, there is no total internal reflection above the second layer, the difference between reflectivities of sastrugi over layered snow and smooth surface over layered snow is not as obvious as in Fig. 13.

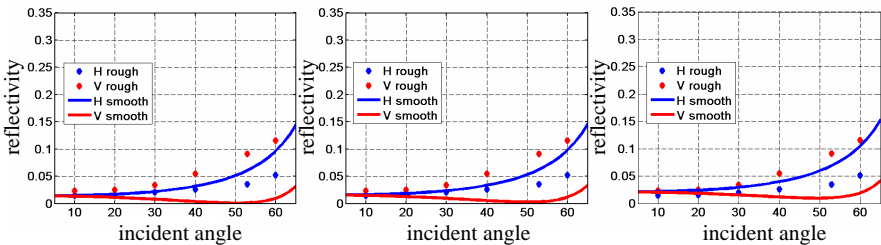


**Figure 14.** Reflectivity of Fig. 12(b) and smooth surface over the same layered snow. Kappa is left:  $1e-10/cm$ , center:  $1e-3/cm$ , right:  $5e-3/cm$ .

In Fig. 15, we plot the reflectivity of profile Fig. 12(c) and the reflectivity of smooth surface case. We can see when incident angles are larger than 50 degrees, the reflectivity of sastrugi over layered snow is obviously larger than the smooth surface case, but smaller than Fig. 13. Compare the figures in Fig. 15 we note that the reflectivity decreases as the absorption increases. And  $H$  channel decreases faster than  $V$  channel. Compare Fig. 13 and Fig. 15, we get reflectivity decreases as the permittivity contrast decreases.

Figure 16 shows the reflectivity of profile Fig. 12(d) and the reflectivity of smooth surface case. When incident angles are larger than 50 degrees, the reflectivity of sastrugi over layered snow is obviously larger than the smooth surface case, and also larger than

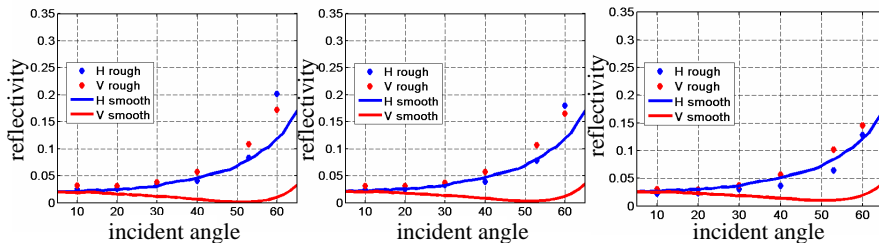


**Figure 15.** Reflectivity of Fig. 12(c) and smooth surface over the same layered snow. Kappa is left:  $1e-10/cm$ , center:  $1e-3/cm$ , right:  $5e-3/cm$ .

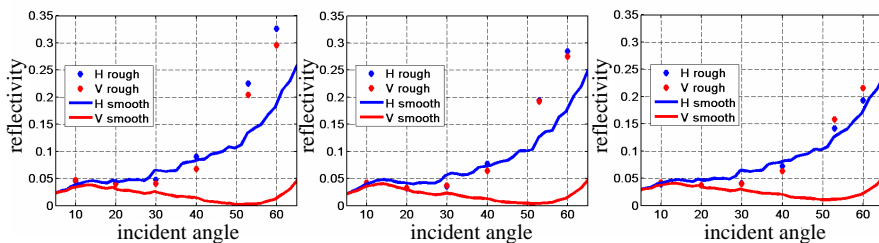


**Figure 16.** Reflectivity of Fig. 12(d) and smooth surface over the same layered snow. Kappa is left:  $1e-10/cm$ , center:  $1e-3/cm$ , right:  $5e-3/cm$ .

reflectivity of sastrugi in Fig. 13 because of more layers. Reflectivity decreases as absorption increases. *H* channel decreases faster than *V* channel.

Figures 13 to 16 show that polarization difference for sastrugi over layered snow is smaller than that of smooth surface over layered snow.

## 7. CONCLUSIONS

The reflectivity of sastrugi over layered snow can be significantly larger than the reflectivity of smooth surface over the same layered snow when 1) sastrugi has large slope and large height and 2) a subsurface layer of snow has smaller permittivity than the surface layer. These two conditions provide the necessary structure for total internal reflection and the significant increase of reflectivity. The analysis in this paper is performed using roughness boundary conditions as derived by surface integral equations for a 2D problem. These boundary conditions are used in mult-layer radiative transfer equations. We show that

rough surface interaction with layered media significantly increases reflectivity and decreases emissivity. This is in contrast to half space problem when rough surface increases emissivity. We are presently extending the analysis to 3D problems and the study of all four Stokes parameters in passive microwave remote sensing.

## REFERENCES

1. Albert, M. R. and R. Hawley, "Seasonal changes in snow surface roughness characteristics at summit, Greenland: Implications for snow and firn ventilation," *Ann. Glaciol.*, Vol. 35, No. 1, 510–514, Jan. 2002.
2. Li, L., P. Gaiser, M. R. Albert, D. G. Long, and E. M. Twarog, "WindSat passive microwave polarimetric signatures of the Greenland ice sheet," *IEEE Trans. on Geoscience and Remote Sensing*, Vol. 46, No. 9, 2622–2631, Sep. 2008.
3. Tsang, L., P. Xu, and K. S. Chen, "Third and fourth stokes parameters in polarimetric passive microwave remote sensing of rough surfaces over layered media," *Microwave and Optical Technology Letters*, Vol. 50, No. 12, 3063–3069, Dec. 2008.
4. Tsang, L., D. Chen, P. Xu, Q. Li, and V. Jandhyala, "Wave scattering with UV multi-level partitioning method part I: 2D problem of PEC surface scattering," *Radio Science*, Vol. 39, No. RS5010, 2004.
5. Domine, F., A. Cabanes, and L. Legagneus, "Structure, microphysics and surface area of the Arctic snowpack near Alert, during the ALERT2000 campaign," *Atmospheric Environment*, Vol. 36, 2753–2765, 2002.
6. Lytle, V. I. and K. C. Jezek, "Dielectric permittivity and scattering measurements of Greenland firn at 26.5–40 GHz," *IEEE Trans. on Geoscience and Remote Sensing*, Vol. 32, No. 2, 290–295, March 1994.
7. Xu, P. and L. Tsang, "Bistatic scattering and emissivities of lossy dielectric surfaces with exponential correlation functions," *IEEE Trans. on Geoscience and Remote Sensing*, Vol. 45, No. 1, 62–72, Jan. 2007.